Towards Improving Wet-Adhesion in a Metal Oxide-Polymer Coating System

Sheila Devasahayam

Steel Institute, University of Wollongong, Northfields Avenue, Wollongong, New South Wales 2522

Received 22 May 2005; accepted 26 July 2005
DOI 10.1002/app.22759
Published online in Wiley InterScience (www.interscience.wiley.com).

ABSTRACT: An investigation using a variable radius roll adhesion test (VaRRAT) revealed an irreversible increase in the wet-adhesion in a metal–oxide–polymer system, under specific experimental conditions. This observation is further confirmed by the T_g measurements and the ATR-FTIR studies. The increase in wet-adhesion is attributed to late H_2O-catalyzed curing of the previously partially cured polymers (epoxy ring opening), as well as the formation of nanocomposite layer within the epoxy primer matrix, because of precipitation of the nanocrystals including zinc ammine complexes formed as a result of dissolution of the zinc/aluminum alloy as well as the metal oxide pigments by the amine crosslinker. High activation energy of ~100 kJ mol^{-1} indicated a chemical process to be responsible for the adhesion gain. © 2006 Wiley Periodicals, Inc. J Appl Polym Sci 99: 3318–3327, 2006

Key words: coatings; adhesion; interfaces; glass transition; FT-IR; activation energy; pigments

INTRODUCTION

A paint–metal system deteriorates upon prolonged exposure to water. Water with dissolved oxygen and ions causes reduction in interfacial toughness, delamination, and corrosion in a paint system. Coatings for a metal system must provide necessary protection against weathering (moisture protection) and corrosion. Inert barriers such as paint or epoxy coating inhibit corrosion by preventing moisture from reaching the metal surface. Unfortunately, coatings have a history of failure because they are often applied improperly, resulting in pinholes and cracks, which will promote crevice corrosion.

The water absorption and water vapor transmission of a coating depend upon the paint system. Presence of hydrophilic and nonionic groups on the polymer skeleton or as additives would result in high water absorption of the paint system. The number of available functional groups and the water uptake in the paint systems are determined by the extent of cure in the paint systems. It is reported that for an epoxy system, water uptake increases with the extent of cure.[1] However, an undercured epoxide system is reported to result in a loss in the interfacial toughness.[2]

H-bonding is the major chemical interaction at the polymer–metal interface in an epoxy–metal oxide system. H-bonding that occurs between the epoxy resin and the steel surface is reported to have little resistance against the water and the alkaline environment.[3] The bond energy[4] for these weak secondary organic film/oxide bonds is less than 25 kJ mol^{-1}. On the other hand, the affinity for water to the polar high-energy iron oxide surface[5,6] is around 40–60 kJ mol^{-1}.

Moisture is reported to cause reduction in the glass-transition temperature (T_g) by plasticizing the polymer network, thus affecting the mechanical performance and durability of the coating system depending upon the hygrothermal history.[7] Since the interfacial strength between the polymer and the metal oxide is related to the mechanical properties of a polymer film, moisture through its action of plasticization affects the adhesion between the polymer network and the metal oxide.

Two distinct categories of water-related deterioration of epoxy composites are reported: (1) mechanical losses due to moisture induced (bound water) plasticization and (2) losses due to moisture-induced (free water) mechanical damage, specifically micro cracking or crazing.[8–10] Losses due to moisture induced plasticization are generally reversible. However, deterioration in the properties due to mechanical damage, chemical reactions, or chain scissions is irreversible.[11]

The present study explores the changes that occur in a paint–metal oxide coating system due to prolonged exposure to water under severe conditions. The main objective of the present study is to determine the effect of moisture on long term adhesion and the adhesion-related properties in the primed-only steel. The main focus is from mechanical point of view rather than electrochemical.

Correspondence to: S. Devasahayam (devasahayam@measurement.gov.au).

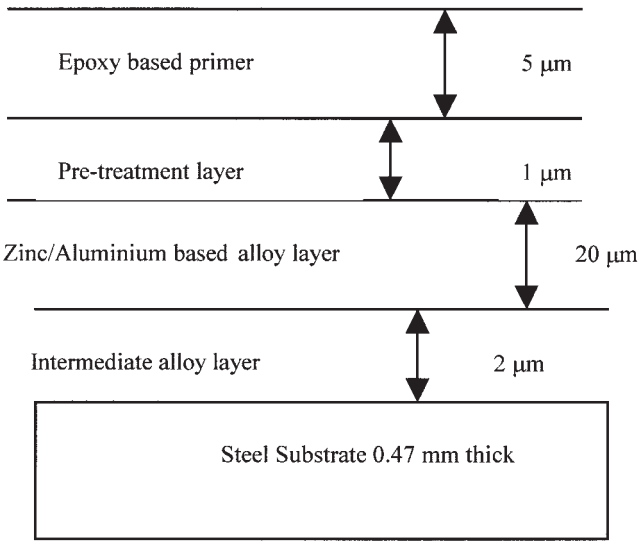

Figure 1 The coating system.

EXPERIMENTAL

Samples

The paint system consists of a metallic substrate of 0.47-mm thick steel sheet, coated with 20 μm of Zinc/Aluminum alloy and 5 μm of epoxy based primer. The primed sample was removed just prior to the application of the topcoat from the continuous paint line process.

The coating system is represented in Figure 1. The structures of the resin used are shown in Figure 2(a) for the epoxy and in Figure 2(b) for butylated urea-formaldehyde, the crosslinker. The epoxide resin used in the present study was produced from bisphenol A and epichlorohydrin. The typical properties of the resin are as follows: viscosity at 25°C, 5.0–9.0 Pa s; density at 25°C, 1.2 g cc^{-1}; T_g, 80°C; molecular weight, 4000; epoxy group content, 260–390 mmol kg^{-1}; esterifiable group content, 4480 mmol kg^{-1}; and hydroxyl group content, 3800 mmol kg^{-1}. The epoxy resins and the crosslinker are mixed in the ratio of 9 : 1 parts by mass.

The paint panels as received were kept in the QUV/Cleveland for a required time at the experimental temperatures. Moisture was prevented from getting through the edges by sealing the edges off using Silastic 732 (a silicone sealant). The panels were then cut to 300 × 24 mm^2 panels for the adhesion tests.

Reference samples are samples exposed to the experimental temperatures in an oven, but not to moisture.

Weathering tests

The painted panels as received were exposed to a constant condensing humidity of 95% at different temperatures (27, 40, 55, and 68°C) in a QUV accelerated weather tester (in a condensation mode only, i.e., no UV light cycle) and a Cleveland condensation tester, for a required time at the experimental temperatures.

The QUV accelerated weather tester exposes the samples to alternating cycles of light and moisture, at controlled, elevated temperatures. In a few days or weeks, the QUV accelerated weather tester can reproduce damage that occurs over months or years of being outdoors. (The UV-A 340 lamps, not used in the present study, provide the best available simulation of sunlight in the critical, short wavelength region from 315 to 400 nm.) Exposure of tests samples from 0500 hrs to 2000 hrs, provides a good representation of an environment's most detrimental effects on a material.

The Cleveland humidity test, named after the Cleveland Society for Coatings Technology, which developed it, establishes high humidity from a heated water supply in the base of the test cabinet. This test is carried out in accordance with The American Standard, "ASTM D 4585–92 Standard Practice for Testing Water Resistance of Coatings Using Controlled Condensation," and is similar to ISO 6270, in that the test coatings form the cover for the test cabinet; the operating temperature, however, can be adjusted in the range 38–82°C. There must be a temperature differential between the cabinet air temperature and the room temperature of at least 11°C, to ensure that condensation takes place on the test faces.

In the present study, the QUV weather tester was operated in the condensation mode at 55 and 68°C, and Cleveland tester was operated at 27 and 40°C.

Variable radius roll adhesion test

The interfacial toughness of the samples exposed to moisture over a period of time and at different temperatures was calculated from the measured critical

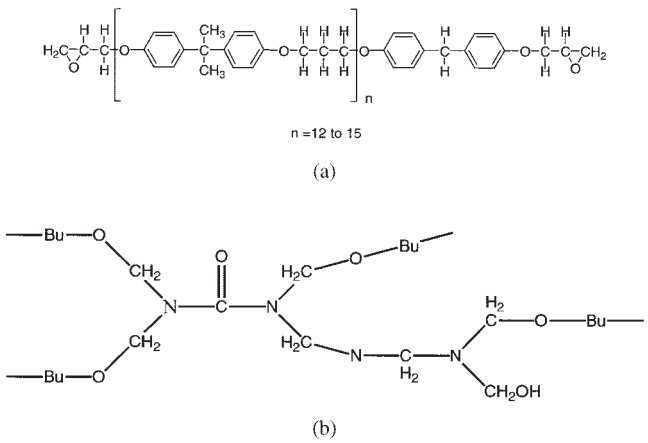

Figure 2 (a) Structure of epoxy resin. (b) Structure of butylated urea–formaldehyde.

radius at room temperature using the variable radius roll adhesion test (VaRRAT).[12] This test relies on the application of a reinforcing layer of epoxy resin over the painted side of a narrow strip of the coated metal. The sample is locked into the roll at the low radius of curvature section and the steel substrate is rolled away from the epoxy resin propagating a crack somewhere within the paint system, or at the metal–primer interface. The loading configuration drives the crack preferentially toward the steel rather than into the epoxy resin. The epoxy resin overlay provided sufficient stiffness to cause the crack to propagate when the steel is rolled around an appropriate radius. The parameters measured were the critical roll radius,* which is a function of the epoxy resin thickness.

Epoxy resin cure: The diglycidyl ether of bisphenol A based epoxy resin used in the present study was Ciba Geigy (two part epoxy) K106. The resin (AW106) to hardener (HV 953U) ratio was 100:80 w/w. The paint panels were then cut to 300 × 24 mm^2 strips for the adhesion tests. The samples were wiped clean with alcohol, and Ciba-Geigy K106 epoxy resin was poured over a casting tray containing the samples and two dog-bone molds. The samples were placed in an oven at 50°C for 24 h. A 50°C cure temperature was used so as to minimize the thermal mismatch stress when the samples cooled because of the differing thermal expansion coefficients of the steel and the epoxy resin. A low temperature cure cycle is not expected to cause additional paint cure or change in the paint properties. Epoxy application and curing conditions were identical for aged and the unaged samples. After curing, the samples were machined to the required dimensions. The adhesive layer thickness varied between 1 and 3 mm. The dog-bone samples, with the dimensions of 100 mm × 13.58 ± 0.14 mm × 2.46 ± 0.04 mm were used to determine Young's modulus of the bulk epoxy resin overlay. Compressive residual stresses of the epoxy over lay measured from the radius of the curvature of the sample were in the order of 5 J m^{-2}. The measurement of mechanical properties of the epoxy overlay was carried out using an Instron 4302 testing machine. The Young's modulus was calculated from the stress–strain curves under uniaxial tension up to a strain of 0.1 at strain rate of 3% min^{-1}.[12] The T_g of the epoxy overlay ranged between 119 and 122°C. Changing the cure conditions will affect the material properties of the epoxy over lay, e.g., Young's modulus.

*Critical radius: The crack propagates around steadily increasing radii until it finds some critical radius at which insufficient energy is stored in the epoxy resin to drive it further. Smaller critical radii represent stronger adhesion energies.

The interfacial toughness is calculated as $G = Gb + Gp$, where Gb is the bending interfacial toughness and Gp is the Poisson's interfacial toughness as given below:

$$G_b = \frac{E^2}{2E_u}\int_0^H \left(\frac{(h_s + 2x/h_s + 2R)}{1 + D(h_s + 2x/h_s + 2R)}\right)^2 dx$$

$$G_p = \frac{E^2}{2E_u}\int_0^H \left(\frac{v(h_s + 2x/h_s + 2R)}{1 + Dv(h_s + 2x/h_s + 2R)}\right)^2 dx$$

where R is critical radius (m); D the shape factor; E the loading modulus (MPa); H the epoxy layer thickness (m); E_u the unloading modulus (MPa); h_s the thickness of the substrate (m); and Poisson's ratio is 0.37. The values of E and E_u were experimentally determined in this study from the stress–strain relationship of the bulk epoxy. D, the shape factor is the fitted parameter obtained using the following classic equation:

$$\sigma = E\frac{\varepsilon}{1 + D\varepsilon}$$

where, σ is stress (Pa) and ε is engineering strain.[12] A change in mechanical properties could affect the G parameter.

T_g measurements

Changes in T_g, ("onset temperature of bulk softening") due to the moisture uptake, were determined by the probe-penetration depth using thermal mechanical analysis (TMA). The measurements were carried out on a Perkin–Elmer TMA-7, operating with a 1-mm diameter hemispherical probe, heating rate of 10°C min^{-1}, and probe force 50 mN under N_2.

ATR-FTIR measurements

The chemical changes occurring in the paint system due to the exposure to moisture were determined using ATR-FTIR in dry-air (Nexus 870, DTGS TEC). Sixty-four scans were taken with 64 background scans at a resolution of 4 cm^{-1}. Ge was used as the ATR crystal.

RESULTS

Adhesion experiments

Failure for the samples exposed to moisture at temperatures of 27 and 40°C was observed at the Zn/Al-based alloy layer/primer interface, i.e., adhesive failure and not within the primer layer, i.e., failure is not due to the cohesive failure. This indicates that the

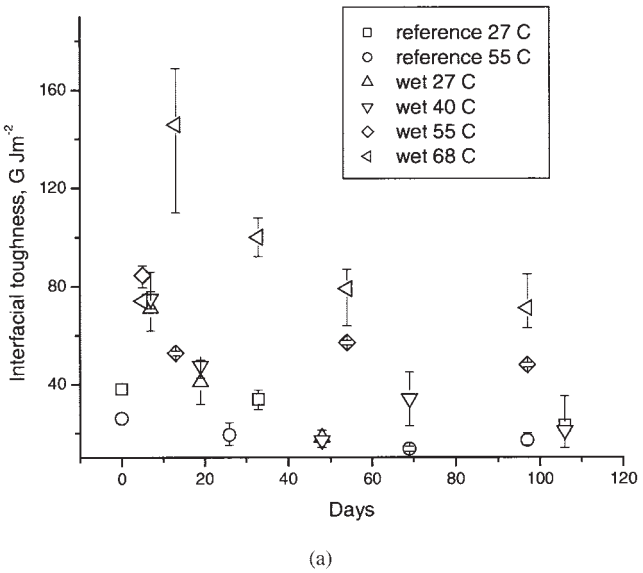

(a)

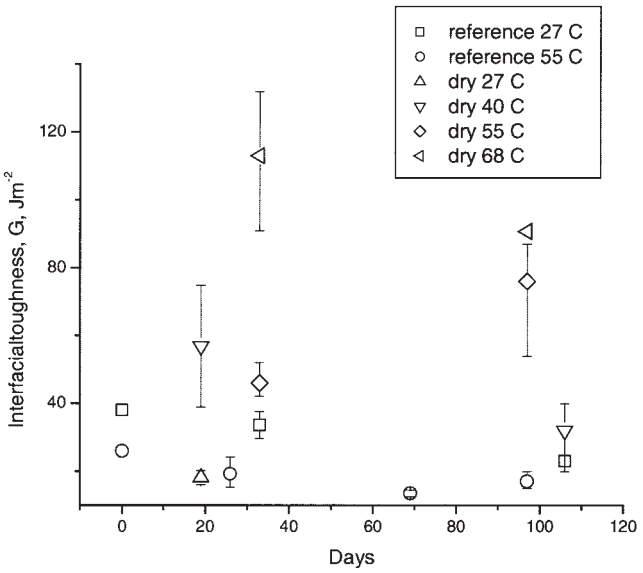

(b)

Figure 3 (a) Effect of moisture on interfacial toughness with respect to time and temperature (reference, samples not exposed to humidity; and wet : samples exposed to humidity). (b) Effect of moisture on interfacial toughness with respect to time and temperature primer (reference, samples not exposed to humidity; and dry : samples allowed to dry naturally after exposure to humidity).

water has permeated through to the Zn/Al-based alloy layer.

Average results of a set of three adhesion experiments, for each sample, are presented in Figures 3(a) and 3(b). Interfacial toughness, *G*, was found to vary with respect to time [Fig. 3(a)] and temperature of exposure to humidity as determined by VaRRAT.[12] *G* corresponds to adhesion energy when the sample exhibits adhesive failure and to cohesive strength when the failure occurs within the primer layer. The samples exposed to the moisture at all the temperatures showed an initial increase in the interfacial toughness compared to the reference samples at 27 and 55°C. For the samples exposed to lower temperatures of 27 and 40°C, the interfacial toughness started to decline with the increasing exposure time. The samples exposed to moisture at 55 and 68°C showed higher *G* values, corresponding to the cohesive strength of these material than the reference samples, and upon drying these samples at ambient conditions [Fig. 3(b)], they did not revert back to their original lower *G* values.

Reference samples

Loss in interfacial toughness, *G*, for reference samples (Figs. 3(a) and 3(b)) is attributed to the loss in volatile products.

Kinetics and mechanisms

The rate constants, *K*, for the loss in interfacial toughness *G* as a function of time is determined by plotting α, the fraction transformed at different temperatures against the time (Fig. 4). *K* was determined from the slopes of these plots.

The fraction transformed is defined by the relation $\alpha = \dfrac{G(0) - G(t)}{G(0)}$ = change in interfacial toughness at time t/interfacial toughness at time zero. *K* is the slope of α versus time curve.

While the plots of α versus time for 55 and 68°C remained linear, indicating a chemical or surface-controlled reaction mechanism, the plots for 27 and 40°C tend to level off rather than remain linear till the end, indicating a change in reaction mechanism at these temperatures, perhaps a diffusion controlled mechanism. *K* was determined for 55 and 68°C from the slopes of α versus time plots.

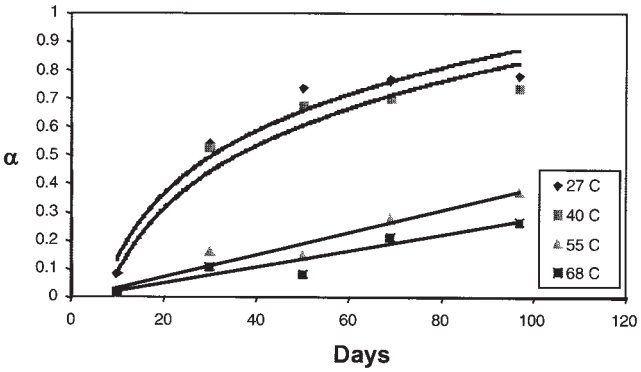

Figure 4 Plot of fraction transformed α versus time for primer samples.

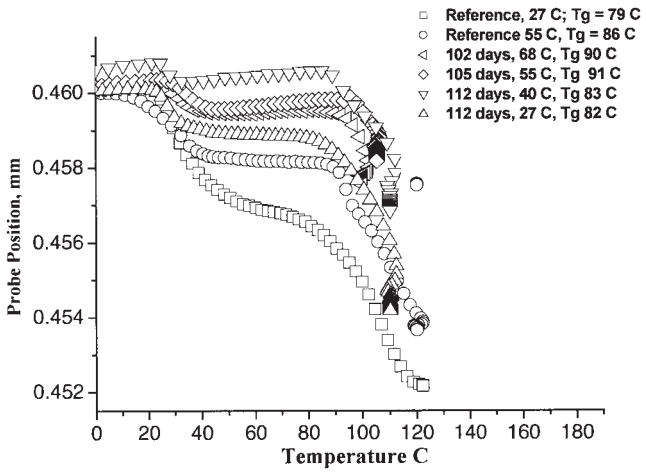

Figure 5 TMA curves of the primer samples exposed to moisture.

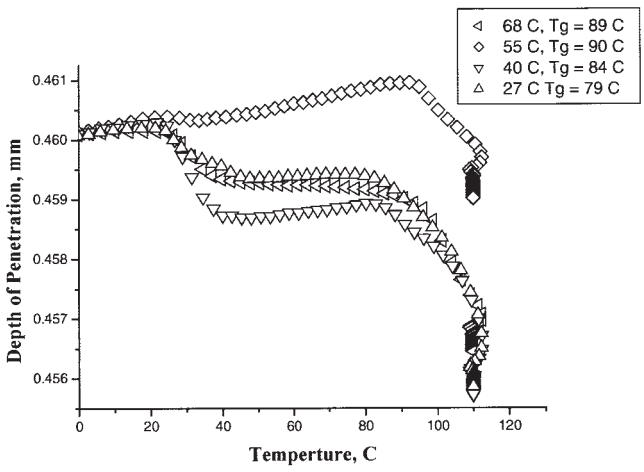

Figure 6 TMA curves of the "dry" primer samples.

Activation energy was determined from the K values of 55 and 68°C to be 100 kJ mol^{-1}using eq. (1).

$$\log\frac{K_2}{K_1} = \frac{E_a}{2.303R}\left(\frac{T_2 - T_1}{T_2T_1}\right) \quad (1)$$

The activation energy for 27 and 40°C was determined to be 31 kJ mol^{-1}using differential approaches without reference to any particular kinetic model (eqs. (2) and (3)). According to eq. (2), $t(\alpha)$, the time required for a fixed α is directly proportional to $\exp(E_a/RT)$.[13] Plot of $t(\alpha)$ versus $1/T$ for different α values yields the activation energy. However, because of lack of enough data, the activation energy was calculated using eq. (3).

$$t(\alpha) = \frac{\text{const.}}{A}\ \exp(E_a/RT) \quad (2)$$

$$\log\frac{t_2(\alpha)}{t_1(\alpha)} = \frac{E_a}{2.303R}\left(\frac{T_2 - T_1}{T_2T_1}\right) \quad (3)$$

TMA measurements

The samples were subjected to humidity effects below the glass-transition temperature of the primer layer. The T_g of the primer sample as received was 80°C. The TMA curves for primer showed two transitions (Fig. 5), a smaller transition around 23°C and a major transition around 80°C. The smaller transition is due to the excess crosslinker present. The major transition is attributed to the T_g of the epoxy resin. Samples exposed to the moisture at 27 and 40°C showed no change in the T_g. The samples exposed to moisture at 55 and 68°C showed an increase up to 10°C in the T_g (major transition). The reference samples at 27 and 55°C showed only a slight increase in the T_g. Upon drying the samples under ambient conditions, the T_g of these samples did not revert back to original values as can be seen from Figure 6. The changes that had occurred appear to be permanent under these conditions. Table I shows the changes in major transition observed. It is worthwhile to notice that the depth of penetration for the samples aged in water at high temperature is even less (though slightly) than the samples as received.

ATR-FTIR

FTIR studies were carried out to establish if any chemical changes took place in the paint system because of prolonged exposure to moisture. Figures 7(a) and 7(b) show the ATR spectra of the samples exposed to moisture at 55°C for 97 days (55°C wet), and subsequently allowed to dry naturally (55°C dry), and the reference sample at 27°C (reference sample 27°C). Changes are observed in the CH_2 region 2965 and 2928 cm^{-1} due to the methylene bridges occurring during condensation of urea–formaldehyde crosslinker (Fig. 8) and due to the epoxy-ring opening.

Figure 7(b) indicates that there is still some unreacted epoxide group (907 cm$^{-1)}$ present in the reference sample at 27°C. However, the intensity of the epoxide peak at 907 cm^{-1} is found to diminish upon exposure to moisture. Changes are also seen in the ether region 1040 and 1073 cm^{-1}, indicating the for-

TABLE I
Observed Changes in T_gs

Temperature (°C)	T_g (°C)			
	As received	References	Wet	Dry
27	80	79	82	79
40	80	NA	83	84
55	80	86	91	90
68	80	NA	90	89

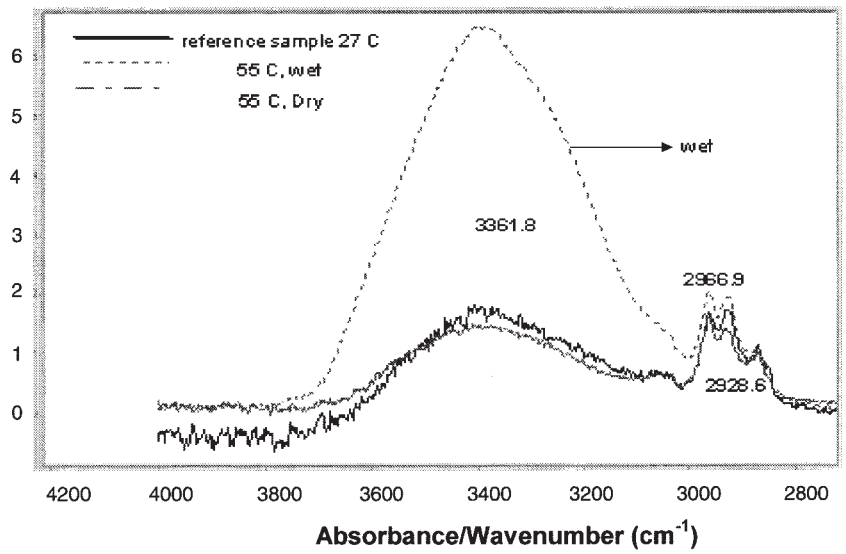

(a)

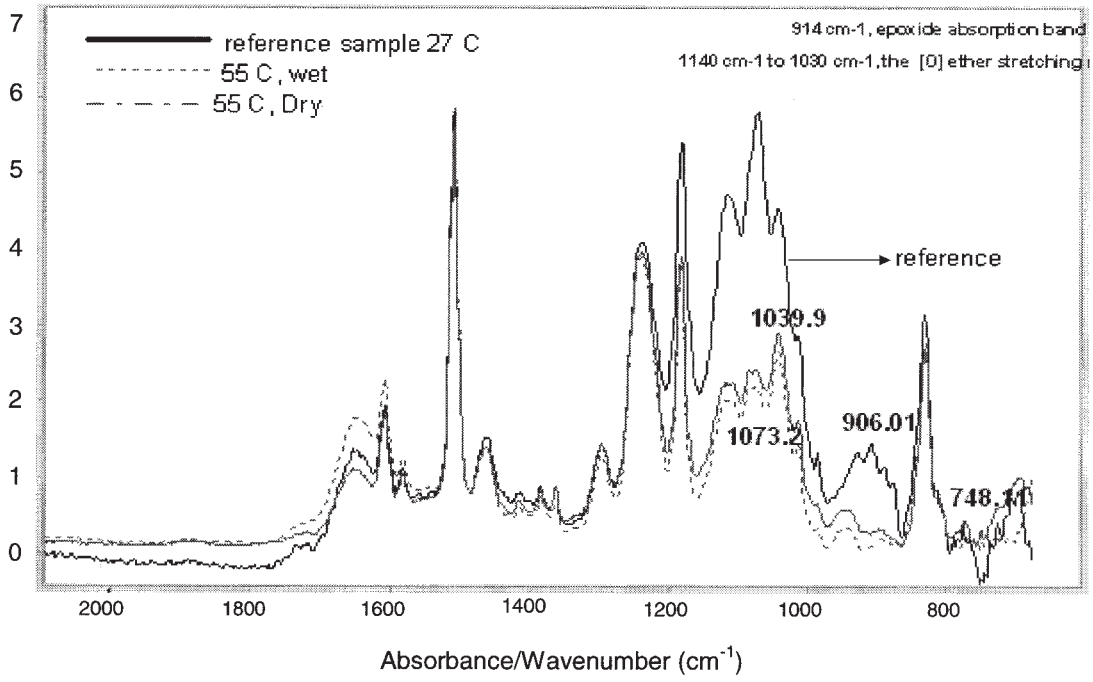

(b)

Figure 7 (a) ATR spectra of primer samples (reference, 27°C; wet, 55°C; dry, 55°C). (b) ATR spectra of primer samples (reference, 27°C; wet, 55°C; dry, 55°C).

mation of a different kind of ether due to the reaction with the epoxide. These reactions appear to be permanent, as upon drying, the chemical changes that have occurred in these samples are still maintained. The FTIR spectra of the dry samples are different from the spectra of the reference samples. It may be concluded that the irreversible increase in the wet-adhesion observed is caused by the permanent chemical changes occurring in these paint systems at high temperatures in water.

DISCUSSION

Initially, this study was carried out with the preconceived notion that the interfacial toughness, G, of a coating system would decline with time upon exposure to the moisture, more so for a system devoid of the topcoat. The primed samples have a thickness of 5 μm as opposed to the topcoat samples with an additional thickness of 18 μm and are expected to be more vulnerable to moisture effects. A decline in T_g was also

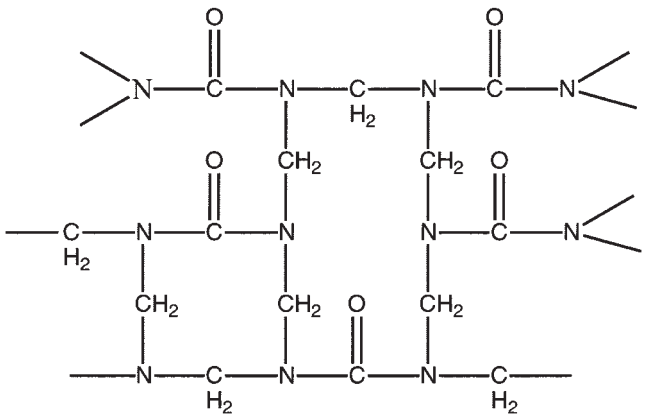

Figure 8 Urea–formaldehyde network with methylene bridges.

expected upon exposure to the moisture. The observed increase in interfacial toughness, *G*, prompted further investigations to be carried out. An irreversible increase in T_g, the permanent chemical changes observed by ATR-FTIR, and the high activation energy confirmed irreversible chemical reactions taking place.

The earlier studies on the metal oxide–paint systems report a decrease in the T_g upon exposure to moisture.[7,11] Loss of mechanical properties in the epoxy resins at elevated temperature enhanced as a result of absorbed moisture has been reported by several workers.[11,14–16]

However, Johncock observed an increase in T_g as a result of water-induced additional cure of incompletely cured epoxy systems.[17] Hashim et al. have reported a moisture-cure of a precured epoxidized natural rubber with aminopropyltriethoxysilane, which resulted in vulcanizates of considerable tensile strength.[18]

The observed increase in interfacial toughness and T_g upon exposure to moisture in the present study suggests an ongoing curing reaction accelerated by moisture as reported by Johncock.[17] As previously mentioned, these are the samples that are removed from the continuous paint line process just prior to the application of the topcoat, with excess epoxy resin and crosslinker meant for further reaction with the topcoat. The interaction between the topcoat and the primer involves the crosslinker in the primer reacting with the resin in the topcoat and *vice versa* at the interface between the topcoat and the primer. Subsequent exposure to the moisture at higher temperatures, for e.g. 55 and 65°C lead to a continued curing (crosslinking) of the unreacted functional groups, resulting in an increase in the T_g. An increase in the T_g due to the crosslinking renders the coating material with better mechanical properties, such as higher modulus and ductile strength. Consequently, the interfacial toughness, *G*, also increases. The reference samples not exposed to moisture at 55°C did not show an increase in interfacial toughness, *G*.

The conventional alcohol-catalyzed cure reactions facilitate the ring opening of the epoxide by forming H-bond with the oxygen in the oxirane ring as shown in Figure 9. Urea–formaldehyde, the crosslinker used in the primer forms ether as shown in Figure 10 in the presence of a catalyst, the butyl alcohol.[19] In the present study, changes seem to occur in the ether

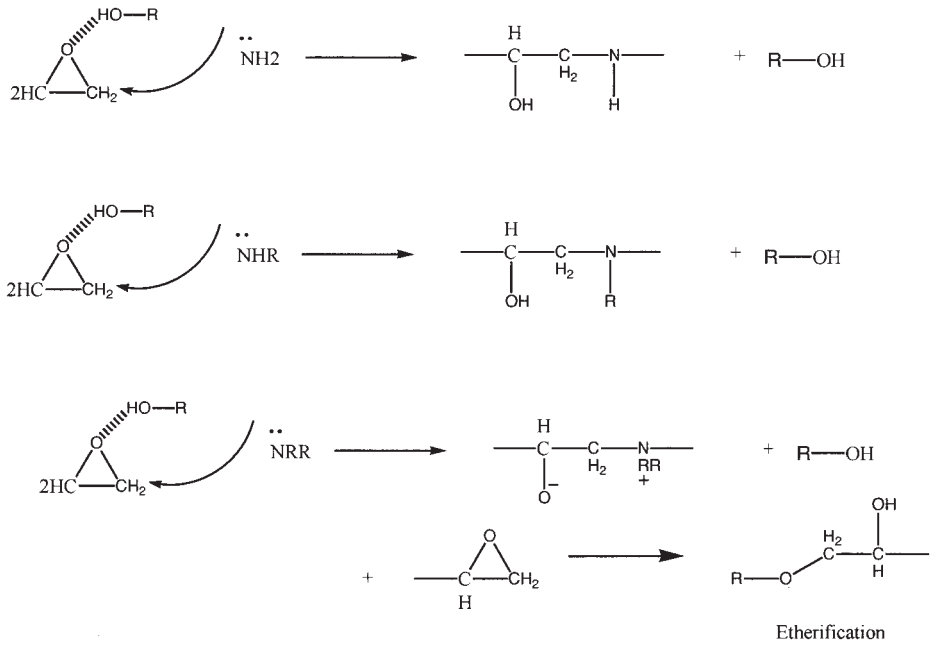

Figure 9 Alcohol-catalyzed crosslinking reaction between epoxy and amines.

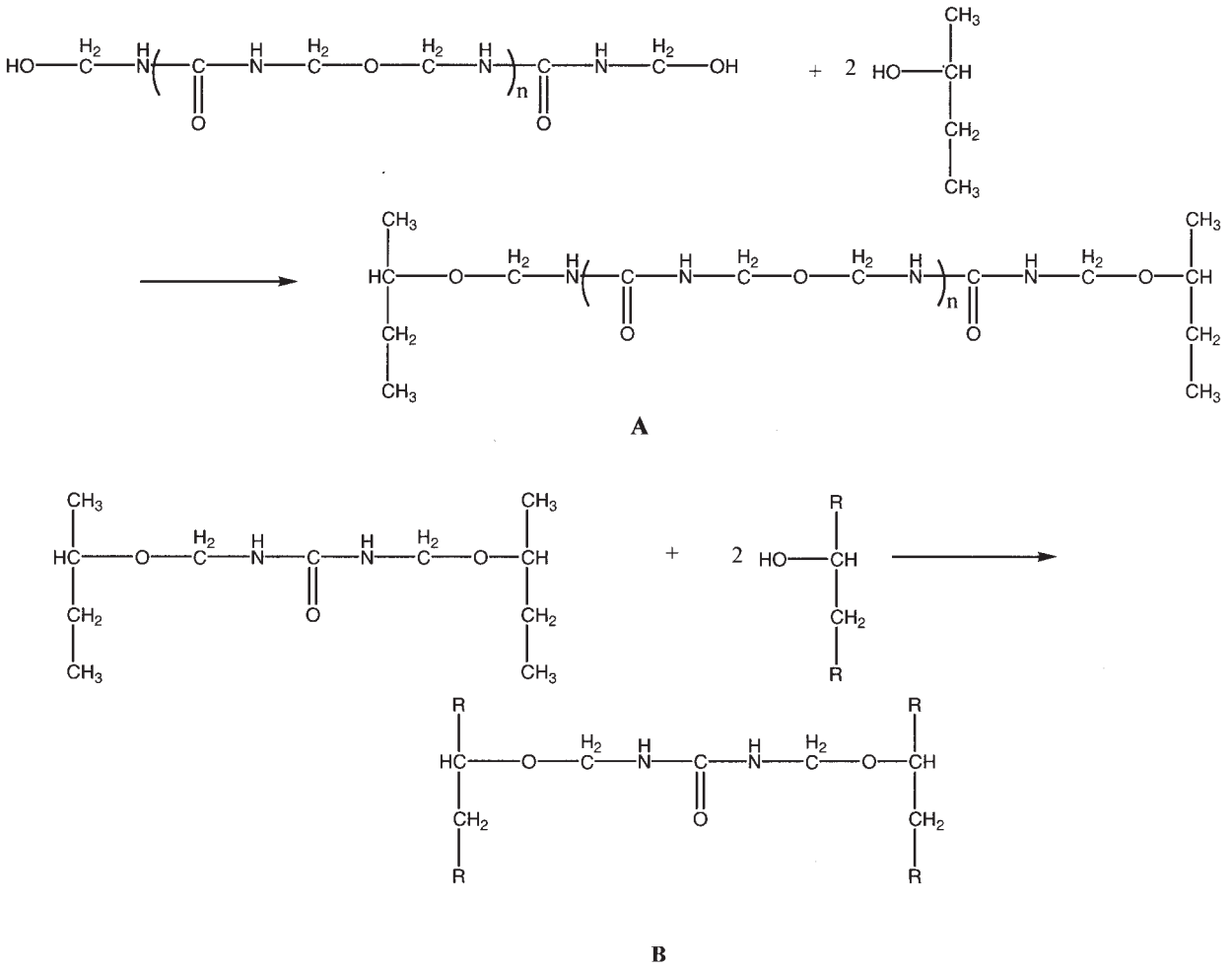

Figure 10 (a) Etherification reaction of butyl alcohol and urea and resulting chemical structure. (b) crosslinking reaction between the urea–formaldehyde and the epoxy resins.[19]

region at 1039 and 1070 cm^{-1}, reflecting water-catalyzed reactions of the crosslinker with epoxide to form different kind of ethers. Decreasing intensity of the epoxide peak at 907 cm^{-1} is a further indication of further curing aided by water via epoxide ring opening.[11]

In addition to inducing additional cure, the absorbed water in the presence of NH_3 favors formation of nano-disperse phase in the primer layer, by mobilizing the metals present in the metallic coatings, resulting in an increased interfacial toughness, *G*, as explained in the following section. The metal ions migrate to the active site on the sample surface to inhibit corrosion attack by precipitating into a protective film, upon exceeding their solubility limit.

The Zinc/Aluminum coating consist of two phases: Al-rich alloy dendrites and Zn-rich alloy phase as reported by Gao et al.[20] A metastable intermetallic phase Al0.71Zn0.29 is formed on the zinc–aluminum coating surface because of the decomposition of the Al–Zn alloy. Al has a much more negative standard electrode potential ($E0 = -1.663$ V) than Zn ($E0 = -0.763$ V).[20,21] However, it is reported that Zn is removed first from the Zn-rich alloy phase because, Al has a strong oxidation tendency in an oxygen-containing atmosphere, and forms a layer of alumina:

$$2Al + 3O_2 = 2Al_2O_3$$

Al_2O_3 is known to be compact and stable. A thin film of Al_2O_3 has a good protective ability to prevent the Al-rich alloy phase from further corrosion. Aluminum oxidizes much slower than iron, because of the formation of aluminum oxide barrier layer, which is a much more effective barrier than the oxide film on iron is. Normally the oxide films with low diffusion coefficients and high melting point form effective barriers. Another factor that determines the barrier property is the electrical resistivity. Electrons passage through the films facilitates oxidation. If the films are insulators, with high electrical resistivities, they exhibit better barrier protections. Because of the high electrical resistivity of Al_2O_3, which is greater than that of FeO, Al_2O_3 shows better barrier properties than FeO.

The Zn-rich phase, on the other hand, does not have the ability to form this type of protective film. When atmospheric oxygen is reduced in the presence of $H^+_{(aq)}$ supplied by H_2CO_3 formed from dissolved CO_2, water, and zinc in Zinc/Aluminum coating, the metal alloy coating is easily oxidized to $Zn(OH)_2$. Zinc hydroxide reacts with the CO_2 in the atmosphere to form a large amounts of tough layer of $Zn(OH)_2{\cdot}xZnCO_{3,}$ the corrosion products, which strongly adheres to the metal surface underneath, protecting it[22] (zinc acts as a sacrificial anode, as it is above the iron in the redox potential table). This layer is reportedly marked with defects, such as cracks and crevices.[23] This would facilitate breaking of adhesion bonds leading to delamination of coating layer. However, in the presence of excess ammonia and OH^-, the corrosion product $Zn(OH)_2$ is dissolved and diffuses into the polymer matrix rather than forming a tough layer between the metal surface and the coating.[22]

With increasing temperatures, the solubility of CO_2 is reduced to a greater extent than the solubility of O_2 and the ratio of CO_2 to O_2 declines. A decrease in CO_2 results in an increase in the pH of an aqueous system. At a higher pH, water can react with the excess crosslinker, urea, present in the primer layer, to produce ammonia and more OH^- ions. This reaction is initially facilitated at high temperatures, because of low solubility of atmospheric CO_2 in water, which raises the pH and imparts basic character to the water, shifting the equilibrium towards right as shown below:[24]

$$H_3O^+ \leftrightarrow H_2O \leftrightarrow OH^-$$

The OH^- reacts with urea as shown below, producing ammonia.[25]

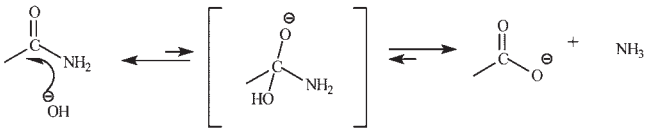

Ammonia can effectively leach out zinc, from zinc–aluminum coating, forming tetra ammine zinc(II) hydroxide tetrahedral complex and chromium from chromium-based pre-treatment layer forming $[Cr(NH_3)]^{3+}$, that are soluble in water.[26,27] The four ammine ligands attached to the Zn can further react with the epoxide via hydrogen bonding. High temperatures and excess ammonia can increase the rate of dissolution and the solubility of these metal complexes. Upon exceeding the solubility limit, the organo zinc complexes will start precipitating out. Aqueous ammonia reacts with aluminum ions also resulting in the formation of a white precipitate, $Al(OH)_3$, which does not redissolve in excess ammonia.

The pigments (made of transition metal oxides) and the fillers present in the primer can also be leached by ammonia. The zinc/aluminum crystallines formed are expected to be of nanoscale and well dispersed as the Ostwald's ripening of the crystals will be minimized due to the surrounding organic matrix.

Ammonia being stronger nucleophile than the water would preferentially bond with Zn to form ammine complex, and the weak base like water may not be able to cleave this bond easily. Because of incorporation of these metal ions into the organic layer, a coating layer comprising nanocomposites, with different mechanical properties, is formed. The metal ion effectively bridges the metal surface and the organic layer because of the increased contacts provided by the multiple ammine ligands attached to metal ions each of which can further react with the oxirane ring via H-bonding. Figure 3(b) shows an increase in the interfacial toughness, *G*, after the dry cycle for the samples exposed to moisture at 55 and 68°C. This could be due to further crystallization caused by the evaporation of water when the solubility product is exceeded. The nano dispersion of the Zn ammine complex and the other crystallines in the polymer matrix would increase the barrier properties, by creating a maze or tortuous path that retards the transport or diffusion of gas molecules or the water molecules through the polymer matrix.[28] Morphology of these crystals could vary from flaky fiber to spindle shaped, depending upon the pH and the nature of the organic matrix.[29,30]

Roche et al.[31–33] have reported dissolution of TiO_2/Alumina during the cure cycle using epoxy diamine monomers. The diamine, the crosslinker, is reported to be responsible for the dissolution reactions. Crystallization of the dissolved/diffused metal oxides within the organic matrix, upon exceeding the solubility product, resulted in increased mechanical properties of the organic matrix. The dissolution and diffusion of the metal ions into the organic matrix lead to interphase formation, resulting in a trilayer system. Further, it is reported that when this trilayer system was aged in water (at 40°C, for 12 h followed by drying at ~20°C and ~50% RH), it showed an increase in the interfacial toughness[33] and this phenomena can be attributed to the formation of needle-shaped organometallic complexes within the polymer matrix acting as a barrier material or water diffusion (corrosion) inhibitor.[32] The barrier properties of the polymer resin are reported to increase with the increasing aspect ratio of the nanocrystals.[28]

A fully cured bi-layer system allowed to age in water showed a decrease in the interfacial toughness.[33,34] This is contrary to what is observed in the present study, where a bi-layer system, when allowed to age in water at high temperatures, shows an increase in the interfacial toughness. However, in the

present study, the bi-layer system is only partially cured. Further cure aided by water and the formation of nanocomposites within the polymer matrix are attributed to the observed increase in the interfacial toughness. It would appear that the size and the shape of Zn crystallites in the nanocomposite layer in the primer matrix are other factors crucial in governing the interfacial toughness.[35] The needle-shaped crystals would increase the longitudinal Young's modulus, thus in turn the interfacial toughness, G.

The activation energies ~30 kJ mol^{-1} for the temperatures 27 and 40°C and ~100 kJ mol^{-1} for the temperatures 55 and 68°C observed in the present study are high for a physical process obeying Henry's law, though activation energy reported for processes such as diffusion is around 36 kJ mol^{-1}, but a high value of ~100 kJ mol^{-1} is indicative of chemical interactions.[36–38]

CONCLUSIONS

Water increases the adhesion in the primed samples at high temperatures. This is attributed to water-aided curing of previously partially cured samples as well as formation of nanocomposite phase within the polymer matrix. Water acts as a catalyst by forming a H-bond with the oxygen in the oxirane ring facilitating ring opening, thus favoring the attack by the nucleophilic Nitrogen.[17]

Ammoniacal leaching of the metal alloy and subsequent diffusion of the metal ions into the organic coating layer produces a coating layer comprising of nanocomposites, with improved mechanical properties than the monomer resins. High temperatures increase the rate of dissolution and the solubility of the organo-complexes. Presence of nanocrystals increases the barrier property by creating a maze or tortuous path that retards the transport or diffusion of gas molecules or the water molecules through the polymer matrix, thus improving the wet-adhesion. The increased T_g, the FTIR studies, and the high activation energies observed are indicative of permanent chemical transformations taking place in the primer layer.

The authors thank Dr. Peter Fredericks, QUT, Australia, for the discussions on ATR-FTIR; Mr. Pat Smith, Bluescope steel, Port Kembla, Australia, for his assistance with Cleveland and QUV; Prof Hugh Brown, University of Wollongong, Australia, for general discussions; and David Buxton, Bluescope Steel Laboratories, Australia, for the research facilities.

References

1. Danieley, N. D.; Long, R. E. J Polym Sci Polym Chem Ed 1981, 19, 2443.
2. Nicodemo, L.; Bellucci, F.; Marcone, A.; Monetta, T. J Membr Sci 1990, 52, 393.
3. MacQueen, R. C.; Granata, R. C. Prog Org Chem 1996, 28, 97.
4. Nguyen, T.; Martin, J. W. Durability of Building Materials and Components; In: Sjosrom, C., Ed.; E & FN Spon: UK, 1996; Vol. 1, p 491.
5. Bolger, J. C.; Michaels, A. S. In: Interface Conversion for Polymeric Coatings; Weiss, P., Cheevers, D., Eds., Elsevier: New York, 1969; p 3.
6. Thiel, P. A.; Madey, T. E. Surf Sci Rep 1987, 7, 211.
7. Choi, H. S.; Ahn, K. J.; Nam, J.-D.; Chun, H. J. Compos Appl Sci Manuf 2001, 32, 709.
8. Browning, C. E. Ph.D. Thesis, University of Dayton, 1976.
9. Browning, C. E.; Husman, G. E.; Whitney, J. M. ASTM Spec Tech Publ 1977, 617, 481.
10. Antoon, M. K.; Koening, J. L. J Macromol Sci Rev Macromol Chem Phys 1980, C19, 135.
11. Netravali, A. N.; Fornes, R. E.; Gilbert, R. D.; Memory, J. D. J Appl Polym Sci 1985, 30, 1985.
12. Jinks, D.; Brown, H.; Buxton, D. J Coat Technol 2002, 74, 49.
13. Ray. H. S.; Kundu, N. Thermochim Acta 1986, 101, 107.
14. Netravali, A. N.; Fornes, R. E.; Gilbert, R. D.; Memory, J. D. J Appl Polym Sci 1984, 29, 311.
15. Netravali, A. N.; Fornes, R. E.; Gilbert, R. D.; Memory, J. D. J Appl Sci 1984, 29, 311.
16. Ellis, T. S.; Karasz, F. E. Polymer 1984, 25, 664.
17. Johncock, P. J Appl Polym Sci 1990, 41, 613.
18. Hashim, A. S.; Kohjiya, S.; Ikeda, Y. Polym Int 1995, 38, 111.
19. Watts, J. F.; Abel, M.; Perruchot, C.; Lowe, C.; Maxted, J. T.; White, R. G. J Electron Spectrosc Relat Phenom 2001, 121, 233.
20. Gao, W.; Gifford, D.; Liu, Z. Y. IPENZ Transactions 1997, 24, No. 1/EMCh.
21. Fontana, M. G. Corrosion Engineering; McGraw-Hill: New York, 1986; p 42.
22. Gillespie, R. J.; Humphreys, D. A.; Baird, N. C.; Robinson, E. A. Chemistry; Allyn and Bacon: Massachusetts, 1985.
23. Reumont, G.; Vogt, J. B.; Iost, A.; Foct, J. Surf Coat Technol 2001, 139, 265.
24. Puri, B. R.; Sharma, L. R. Principles of Physical Chemistry. S. Nagin: Delhi, 1962.
25. Fox, M. A.; Whitesell, J. K. Organic Chemistry; Jones and Bartlett: Boston, 1994.
26. Kazinczy, B.; Kótai, L.; Gács, L.; Szentmihályi, K.; Sándor, Z.; Holly, S. Hungar J Ind Chem 2000, 28, 207.
27. Nakai, T.; Murakami, Y.; Sasaki, Y.; Fujiwara, I.; Tagashira, S. Anal Sci 2004, 20, 235.
28. Ray, S. S.; Okamoto, M. Prog Polym Sci 2003, 28, 1539.
29. Musić, S.; Popović, S.; Maljković, M.; Dragčević, D. J Alloys Compd 2002, 347, 324.
30. Zhu, H. Y.; Riches, J. D.; Barry, J. C. Chem Mater 2002, 14, 2086.
31. Roche, A. A.; Bouchet, J.; Bentadjine, S. Int J Adhes Adhes 2002, 22, 431.
32. Bentadjine, S.; Petiaud, R.; Roche, A. A.; Massardier, V. Polymer 2001, 42, 6271.
33. Bouchet, J.; Roche, A. A.; Jacquelin, E. J Adhes Sci Technol 2002, 16, 1603.
34. Devasahayam, S. J Appl Polm Sci, to appear.
35. Devasahayam, S. J Polym Sci; Part B: Polym Phys 2004, 42, 3822.
36. Marais, S.; Metayer, M.; Nguyen, T. Q.; Labbe, M.; Saiter, J. M. Eur Polym J 2000, 36, 453.
37. Kumar, R. S.; Auch, M.; Ou, E.; Ewald, G.; Jin, C. S. Thin Solid Films 2002, 417, 120.
38. Berry, B. S.; Susko, J. R. Polymer 1977, 21, 176.